Experimental Thermal and Fluid Science 45 (2013) 234–242

Contents lists available at SciVerse ScienceDirect

Experimental Thermal and Fluid Science

journal homepage: www.elsevier.com/locate/etfs

Scale effects affecting two-phase flow properties in hydraulic jump with small inflow Froude number

Hubert Chanson *, Yann Chachereau

The University of Queensland, School Civil Engineering, Brisbane, QLD 4072, Australia

ARTICLE INFO

Article history:
Received 23 May 2012
Received in revised form 27 September 2012
Accepted 10 November 2012
Available online 21 November 2012

Keywords:
Hydraulic jumps
Physical modelling
Dimensional analysis
Scale effects
Air entrainment
Two-phase flows
Bubble clustering

ABSTRACT

The transition from supercritical to subcritical flow is characterised by a strong dissipative mechanism, a hydraulic jump. Herein a comparative analysis of physical data is presented with a focus on a broad range of two-phase flow parameters. The results show that, for hydraulic jumps with $Fr_1 = 5.1$, the void fraction data obtained with $Re < 4 \times 10^4$ could not be scaled up to $Re = 1 \times 10^5$. Most air–water flow properties measured with Reynolds numbers up to 1.25×10^5 could not be extrapolated to large-size prototype structures without significant scale effects in terms of bubble count rate, turbulence, bubble chord time distributions and bubble cluster characteristics. The findings have some implications of civil and sanitary engineering designs, because most hydraulic structures, storm water systems and water treatment facilities operate with Reynolds numbers larger than 10^6 to over 10^8.

1. Introduction

A hydraulic jump is the sudden and rapid transition from a high velocity flow into a slower motion in an open channel [17] (Figs. 1 and 2). It is characterised by some substantial energy losses and air entrapment in the jump roller [21,25]. Fig. 1 presents a hydraulic jump downstream of a dam spillway during a recent flood event and Fig. 2A shows a laboratory model. Traditionally, physical hydraulic models are used to optimize a design and to predict the behaviour of prototype flow situations. The model is investigated in a laboratory under controlled conditions, and the model flow conditions are said to be similar to those in the prototype if the model displays similarity of form, motion and forces [17,19]. In most hydraulic structures including hydraulic jump stilling basins, it is impossible to satisfy simultaneously all the dynamic similarities with geometrically-scaled physical models using air and water [4,27,30]. It was recently argued that the notion of scale effects is critically linked with the definition of key parameters [7].

In this contribution, the validity of the Froude similitude is tested for $Fr_1 = 5.1$ with respect to the two-phase flow properties, including the distributions of void fraction, bubble count rate, interfacial velocity, turbulence intensity and integral turbulent time scales, as well as the probability distribution functions of bubble chord times and clustering properties. The comparison is based upon a comparative analysis of geometrically scaled data obtained with the same type of phase detection probes.

2. Dimensional considerations and physical modelling of two-phase flow properties in hydraulic jump

Any fundamental analysis of hydraulic jumps is based upon a large number of relevant equations to describe the two-phase turbulent flow motion. Physical modelling may provide some insights into the flow motion if a suitable dynamic similarity is selected [7,19,23]. For a hydraulic jump, the relevant dimensional parameters include the air and water physical properties and constants, the flume characteristics, the inflow conditions, and the local two phase flow properties. Considering a jump in a smooth horizontal rectangular channel with an inflow depth d_1 and velocity V_1, a simplified dimensional analysis yields:

$$C, \frac{V}{V_1}, \frac{v'}{V_1}, \frac{F\,d_1}{V_1}, \frac{D_{ab}}{d_1}, \frac{N_c\,d_1}{V_1}, \ldots = F\left(\frac{x-x_1}{d_1}, \frac{y}{d_1}, \frac{z}{d_1}, \frac{V_1}{\sqrt{g\,d_1}}, \rho \times \frac{V_1\,d_1}{\mu}, \frac{\rho\,V_1^2\,d_1}{\sigma}, \frac{x_1}{d_1}, \frac{W}{d_1}, \frac{v'_1}{V_1}, \frac{\delta}{d_1}, \ldots\right) \quad (1)$$

where C is the void fraction, V the air–water velocity, v' a characteristic turbulent velocity, F the bubble count rate defined as the number of bubbles detected per second in a small control volume, D_{ab} a characteristic bubble size, N_c the number of bubble clusters per second, x the longitudinal coordinate, y the vertical elevation above the

* Corresponding author. Fax: +61 7 33 65 45 99.
E-mail address: h.chanson@uq.edu.au (H. Chanson).
URL: http://www.uq.edu.au/~e2hchans/ (H. Chanson).

0894-1777/$ - see front matter © 2012 Elsevier Inc. All rights reserved.
http://dx.doi.org/10.1016/j.expthermflusci.2012.11.014

(A)

(B)

Fig. 1. Hydraulic jump stilling basin downstream basin downstream of the Paradise dam spillway on 30 December 2010 on the Burnett River (QLD, Australia) – $Q \approx 6300\ m^3/s$, $W = 335$ m, $Re \approx 2 \times 10^7$ – Flow direction from left to right. (A) General view. (B) Details of the jump roller.

invert, z the transverse coordinate measured from the channel centreline, ρ and μ the water density and dynamic viscosity respectively, σ the surface tension between air and water, x_1 the longitudinal coordinate of the jump toe, W the channel width, v'_1 a characteristic turbulent velocity at the inflow, δ the boundary layer thickness of the inflow (Fig. 2B). Eq. (1) expresses the air–water turbulent flow properties at a position (x,y,z) within the hydraulic jump as functions of the inflow properties, fluid properties and channel geometry using the upstream flow depth d_1 as the characteristic length scale. In the right hand side of Eq. (1), the 4th, 5th and 6th terms are respectively the upstream Froude number Fr_1, the Reynolds number Re and the Weber number We.

In a hydraulic jump, the momentum considerations demonstrate the significance of the inflow Froude number [1,20] and the selection of the Froude similitude derives implicitly from basic theoretical considerations [9,19].

The Froude dynamic similarity is commonly applied in the hydraulic literature [5,17,23] including in the present analysis. The Reynolds number is another relevant dimensionless number because the hydraulic jump is a turbulent shear flow [18,24,28]. Further the Π-Buckingham theorem implies that any dimensionless number can be replaced by a combination of itself and other dimensionless numbers. That is, the Froude, Reynolds or Weber number may be replaced by the Morton number Mo since:

$$Mo = \frac{g\,\mu^4}{\rho\,\sigma^3} = \frac{We^3}{Fr^2 Re^4} \quad (2)$$

Eq. (1) may be rewritten as:

$$C, \frac{V}{V_1}, \frac{v'}{V_1}, \frac{F\,d_1}{V_1}, \frac{D_{ab}}{d_1}, \frac{N_c\,d_1}{V_1}, \ldots = F\left(\frac{x-x_1}{d_1}, \frac{y}{d_1}, \frac{z}{d_1}, \frac{V_1}{\sqrt{g\,d_1}}, \rho \times \frac{V_1\,d_1}{\mu}, \frac{g\,\mu^4}{\rho\,\sigma^3}, \frac{x_1}{d_1}, \frac{W}{d_1}, \frac{v'_1}{V_1}, \frac{\delta}{d_1}, \ldots\right) \quad (3)$$

when the same fluids (air and water) are used in models and prototype as in the present study, the Morton number Mo becomes an invariant and this adds an additional constraint upon the dimensional analysis. Eq. (3) yields:

$$C, \frac{V}{V_1}, \frac{v'}{V_1}, \frac{F\,d_1}{V_1}, \frac{D_{ab}}{d_1}, \frac{N_c\,d_1}{V_1}, \ldots = F\left(\frac{x-x_1}{d_1}, \frac{y}{d_1}, \frac{z}{d_1}, Fr_1, Re, \frac{x_1}{d_1}, \frac{W}{d_1}, \frac{v'_1}{V_1}, \frac{\delta}{d_1}, \ldots\right) \quad (4)$$

Physically it is impossible to fulfil simultaneously the Froude and Reynolds similarity requirements, unless working at full scale. For example, the air entrainment process is adversely affected by significant scale effects in small size models [4,7,27].

The Reynolds number was selected herein instead of the Weber number because the present study focuses on the scaling of prototype hydraulic jumps with Reynolds numbers from 10^6 to in excess of 10^9 (e.g. Fig. 1). For such large flows, surface tension is considered of lesser significance compared to the viscous effects in the turbulent shear regions [2,4,15,30]. Lastly the Froude and Morton similarities imply that $We \propto Re^{4/3}$ (Eq. (2)).

2.1. Methodology

A number of data sets were re-analysed in the present study (Table 1). All data sets were geometrically similar based upon a Froude similitude with undistorted scaling ratio, and the same types of intrusive phase-detection probes were used (Table 1, column 7). The geometric scaling ratio was $L_{scale} = 3.3$ between the largest and smallest series of experiments ($d_1 = 0.04$ and 0.012 m respectively) where L_{scale} is the geometric scaling ratio defined as the ratio of prototype to model dimensions. Note that all the experiments were conducted in hydraulic jumps with partially-developed inflow conditions. The experimental flow conditions were selected as $Fr_1 = 5.1$ with identical upstream distance x_1/d_1 between gate and jump toe, and the two-phase flow measurements were performed in the developing air–water flow region at cross-sections such that $(x - x_1)/d_1$ 15. For $(x - x_1)/d_1 > 15$, the flow aeration (e.g. void fraction, bubble count rate) was drastically reduced at the lowest Reynolds numbers and the two-phase flow properties could not be recorded with the phase-detection probe technique.

Importantly all experimental data sets were collected in similar facilities, with the same type of instrumentation as well as signal processing techniques. A broad range of air–water flow parameters were systematically tested, including velocity, turbulence, integral time scale and bubble clustering data analyses. The latter data sets were never analysed in terms of dynamic similarity to date. Lastly the range of re-analysed data sets spanned over a wider range of Reynolds numbers (i.e. an order of magnitude herein) than any previous studies;

3. Basic results

In the jump roller, the vertical distributions of void fraction presented a local maximum in the turbulent shear layer while the distributions of bubble count rate exhibited a sharp maximum in the shear region (Fig. 2B). Both features are sketched in Fig. 2B and seen in Fig. 3. Typical comparative results are presented in Figs. 3 and 4 in terms of void fraction and bubble count rate. The physical data showed drastic scale effects in the smaller hydraulic jumps in terms of void fraction and bubble count rate distributions. The results highlighted consistently a more rapid de-aeration of the jump

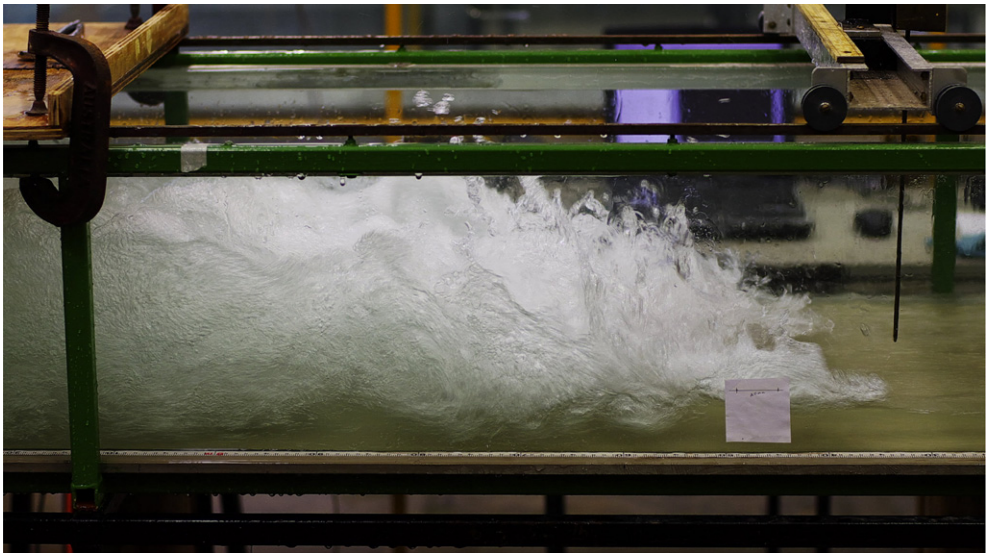

(A)

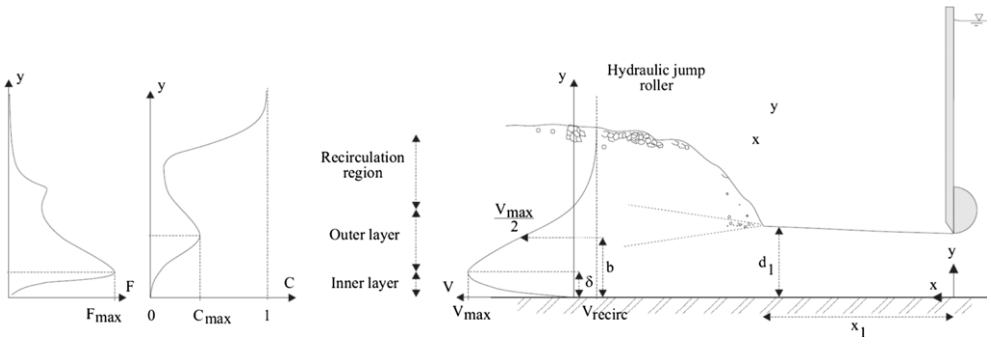

(B)

Fig. 2. Air entrainment in a breaking hydraulic jump. (A) $d_1 = 0.0395$ m, $Fr_1 = 5.1$, $Re = 1.3 \times 10^5$, shutter speed: 1/100 s – Flow from left to right. (B) Definition sketch, including vertical distributions of void fraction C, bubble count rate F and interfacial velocity V in the jump roller.

Table 1
Physical modelling of air–water flow properties in hydraulic jumps at relatively small Froude numbers based upon an undistorted Froude similitude with air and water.

Reference	W (m)	x_1 (m)	d_1 (m)	Fr_1	Re	Instrumentation	$x - x_1$ (m)	C_{max}	F_{max} (Hz)
Chachereau and Chanson [3]	0.50	1.5	0.0395	5.1	1.3×10^5	Dual-tip conductivity (∅ 0.25 mm) sampling: 20 kHz for 45 s	0.150	0.203	106.8
							0.300	0.192	87.2
							0.450	0.070	56.9
							0.600	0.050	40.0
Chanson and Gualtieri [12]	0.50	1.0	0.024	5.1	6.8×10^4	Single-tip conductivity (∅ 0.35 mm) sampling: 20 kHz for 45 s	0.100	–	107.7
							0.200	0.279	80.9
							0.300	0.159	61.1
Murzyn and Chanson [22]	0.50	0.75	0.018	5.1	3.8×10^4	Dual-tip conductivity (∅ 0.25 mm) sampling: 20 kHz for 45 s	0.075	0.218	55.4
							0.150	0.175	43.2
							0.225	0.063	25.4
Chanson and Gualtieri [12]	0.25	0.5	0.012	5.1	2.5×10^4	Single-tip conductivity (∅ 0.35 mm) sampling: 20 kHz for 45 s	0.020	–	46.4
							0.050	–	35.5
							0.100	–	–
Chanson [6]	0.25	1.0	0.024	5.0	7.7×10^4	Single-tip conductivity (∅ 0.35 mm) sampling: 20 kHz for 45 s	0.040	0.364	166.6
							0.100	0.227	77.0
							0.200	0.168	56.7

Note: Hydraulic jumps with partially-developed inflow conditions; all experiments performed with tap water; C_{max}: maximum void fraction in the shear layer; F_{max}: maximum bubble count rate in the shear layer; W: channel width; (–): data unavailable.

roller with decreasing Reynolds number for a given inflow Froude number for Re < 68,000, an absence of self-similarity of the void fraction profiles in the turbulent shear layer for Re < 40,000 (Fig. 3A), and an increasing dimensionless bubble count rate with

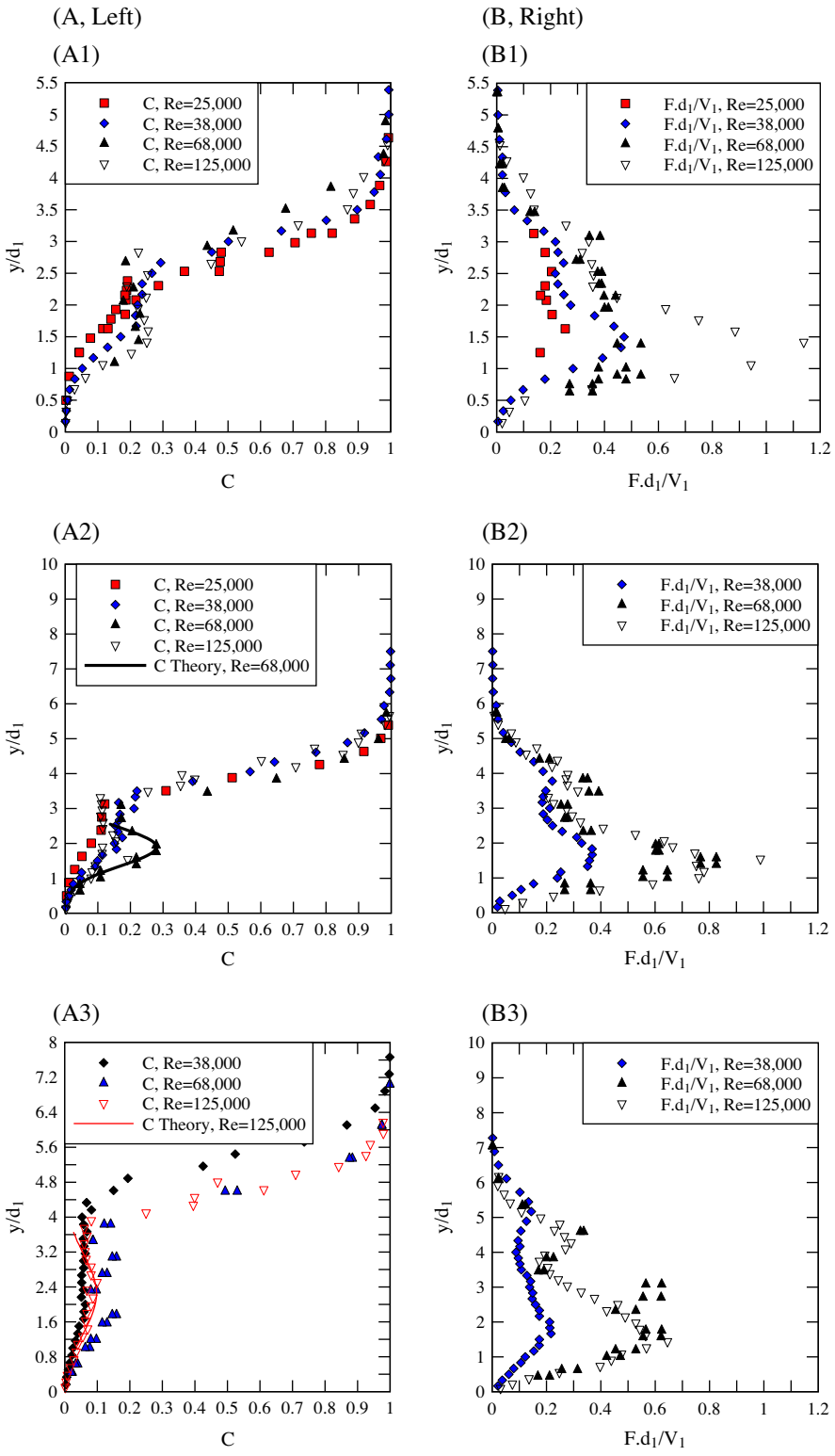

Fig. 3. Dimensionless distributions of void fraction and bubble count rate in the hydraulic jump for $Fr_1 = 5.1$, $x_1/d_1 = 42$, $W/d_1 \geqslant 12$ and Re = 25,000, 38,000, 68,000 and 125,000. (A, Left) Void fraction data. (A1) $(x - x_1)/d_1 = 4$. (B, Right) Bubble count rate data. (B1) $(x - x_1)/d_1 = 4$. (A2) $(x - x_1)/d_1 = 8$. (B2) $(x - x_1)/d_1 = 8$. (A3) $(x - x_1)/d_1 = 12$. (B3) $(x - x_1)/d_1 = 12$.

increasing Reynolds number for a given inflow Froude number (Fig. 3B). In Fig. 3A, the void fraction profiles in the air–water shear layer followed an analytical solution of the air bubble advection equation (Eq. (2)) for Re = 125,000 and 68,000 but were basically flat for Re = 25,000 and 38,000. In a hydraulic jump, the impingement point acts as a localised source of air entrainment and a solution of the air bubble entrainment equation is [8]:

$$C = \frac{\frac{q_{air}}{q}}{\sqrt{4\ \pi\ D^{\#}\ X'}} \times \left(\exp\left(-\frac{\frac{(y'-1)^2}{X'}}{4D^{\#}} \right) + \exp\left(-\frac{\frac{(y'+1)^2}{X'}}{4\ D^{\#}} \right) \right) \quad (5)$$

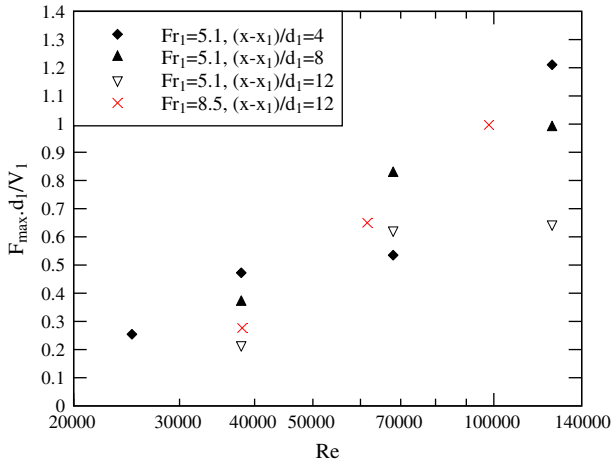

Fig. 4. Effects of the Reynolds number on the maximum void bubble count rate $F_{max}d_1/V_1$ in the turbulent shear layer.

where $X' = (x + u_r/V_1\, y)/d_1, y' = y/d1, u_r$ is the bubble rise velocity, and $D^{\#}$ is a dimensionless diffusion coefficient. Eq. (5) is restricted to the air–water shear layer and it is compared with experimental data in Fig. 3.

The vertical distributions of bubble count rate showed a maximum in the shear region (Figs. 2B and 3). The dimensionless maximum bubble count rate data are summarised in Fig. 4 as functions of the Reynolds number Re. The results highlighted a monotonic increase in maximum bubble count rate $F_{max}d_1/V_1$. No asymptotic trend was observed within the range of investigated flow conditions (Fig. 4). This is illustrated in Fig. 4 showing the dimensionless maximum bubble count rate in the air–water shear layer as a function of the Reynolds number for several dimensionless longitudinal locations. The data highlighted a monotonic trend as well as the absence of an asymptotic limit, demonstrating some scale effects in terms of bubble count rates.

The velocity distribution followed closely a self-similar profile which was close to a wall jet velocity distribution, as discussed by Rajaratnam [24] and Chanson and Brattberg [11]. The results for Re = 38,000 and 130,000 highlighted the self-similarity (Fig. 5A). A relevant parameter is the shear layer thickness, although its quantitative estimate is not trivial. Based upon the velocity profile data, the mixing zone may be conceptualised as a boundary layer region, or inner layer, where $0 < V < V_{max}$ with V_{max} the maximum velocity in a cross-section, and a shear zone, or outer layer, above [16,26]. Such a model is sketched in Fig. 1B using the terminology introduced by George et al. [16] based upon similarity considerations. Although

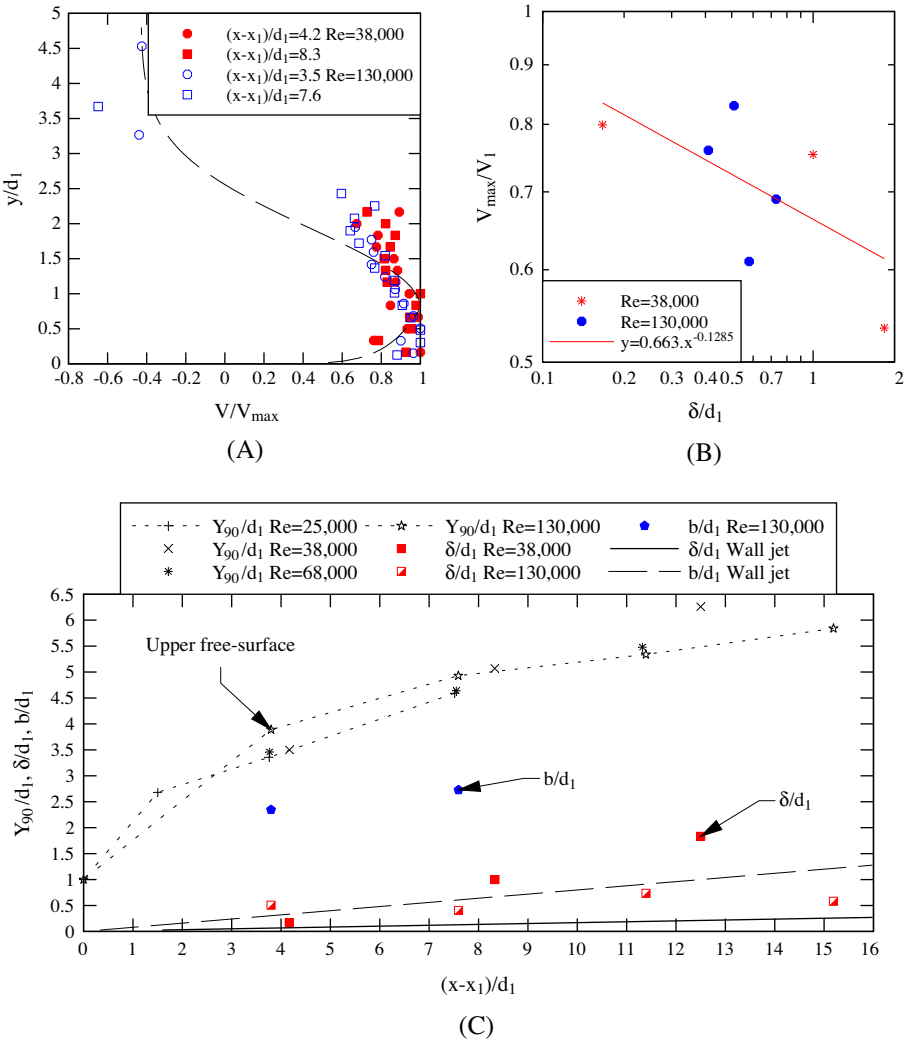

Fig. 5. Interfacial velocity profile in the hydraulic jump roller. (A) Vertical distributions of interfacial velocity for $3.5 < (x - x_1)/d_1 < 8$ – Comparison with the wall jet equations for $(x - x_1)/d_1 = 3.5$ and Re = 130,000. (B) Dimensionless relationship between the maximum velocity V_{max} and inner layer thickness δ – Comparison with Eq. (6). (C) Longitudinal distribution of the inner layer thickness and length scale b (sketch above) defined as the elevation where $V = V_{max}/2$ - Comparison with the roller upper surface elevation Y_{90} and monophase wall jet data [16,29].

there is no theoretical justification, the maximum velocity V_{max} in a wall jet may be normalised in term of the outer layer length scale [16,29]. Herein it is proposed to link the maximum velocity with the inner layer thickness which characterise the vertical extent of the boundary shear stress. The present data are shown in Fig. 5B and the (limited) data set followed a power law trend:

$$\frac{V_{max}}{V_1} = 0.663 \times \left(\frac{\delta}{d_1}\right)^{-0.128} \quad (6)$$

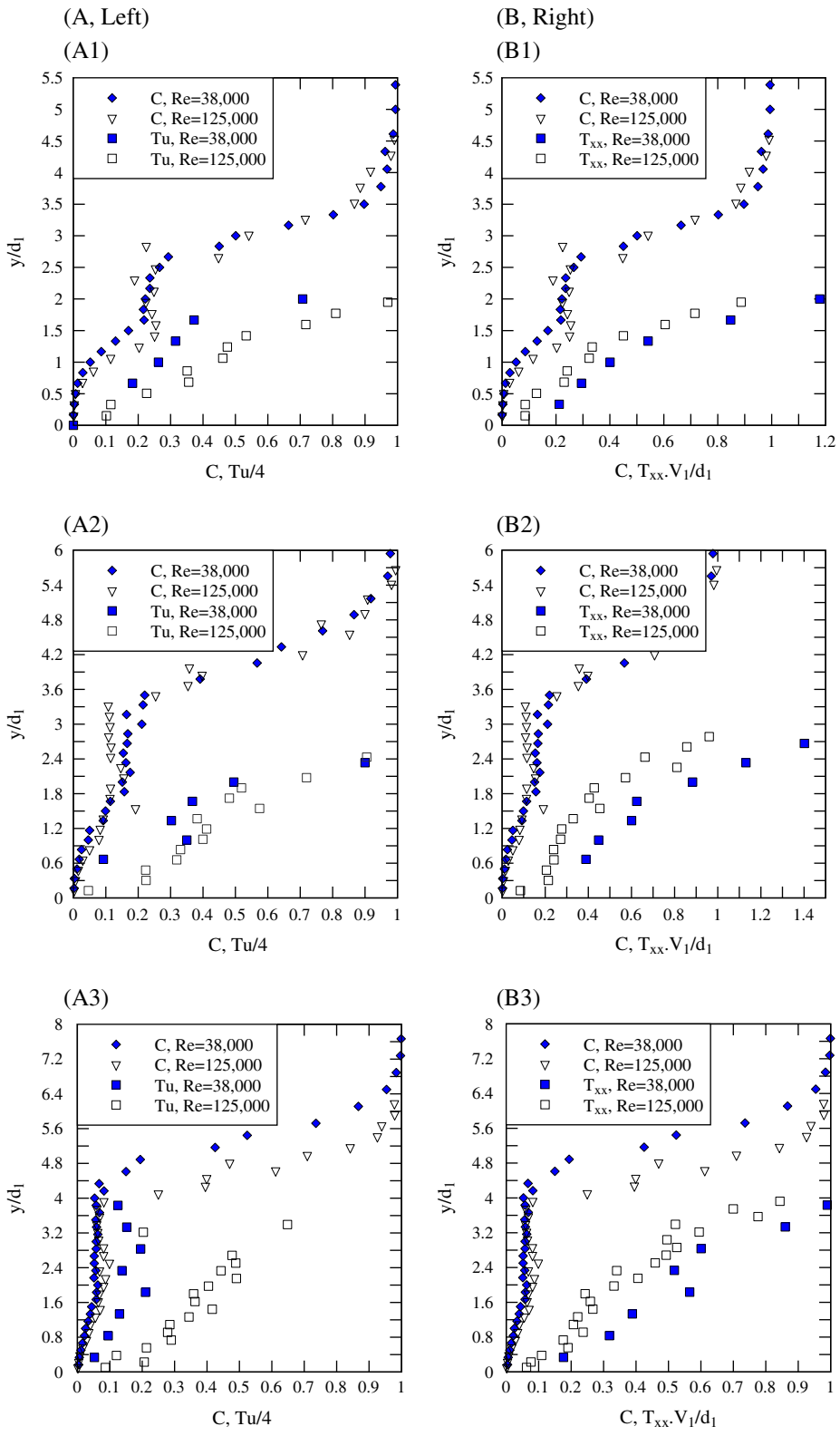

Fig. 6. Dimensionless distributions of void fraction, turbulence intensity and integral time scale in the hydraulic jump for $Fr_1 = 5.1$, $x_1/d_1 = 42$, $W/d_1 \geqslant 12$ and Re = 38,000 and 125,000. (A, Left) Turbulence intensity data. (B, Right) Integral time scale data. (A1) $(x - x_1)/d_1 = 4$. (B1) $(x - x_1)/d_1 = 4$. (A2) $(x - x_1)/d_1 = 8$. (B2) $(x - x_1)/d_1 = 8$. (A3) $(x - x_1)/d_1 = 12$. (B3) $(x - x_1)/d_1 = 12$.

Re	y/d_1	C	$F_{max}d_1/V_1$	N_{ab}
25,000	1.44	0.115	0.25	1598
38,000	1.50	0.170	0.47	2491
68,000	1.76	0.334	1.10	2252
125,000	1.24	0.203	1.33	4804

Re	y/d_1	C	$F_{max}d_1/V_1$	N_{ab}
38,000	1.67	0.058	0.22	1144
68,000	2.42	0.159	0.62	900
125,000	1.24	0.079	0.71	2561

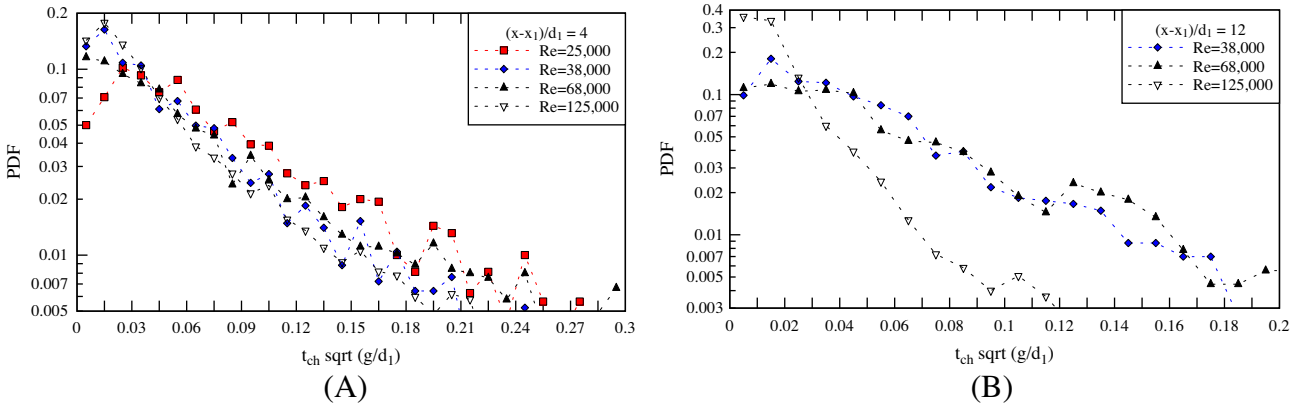

Fig. 7. Dimensionless probability distribution functions of bubble chord time $t_{ch}\sqrt{g/d_1}$ in the developing shear layer of hydraulic jumps at $F = F_{max}$ for $Fr_1 = 5.1$, $x_1/d_1 = 40$, $B/d_1 \geqslant 10$ and Re = 25,000, 38,000, 68,000 and 125,000. (A) $(x - x_1)/d_1 = 4$. (B) $(x - x_1)/d_1 = 12$.

Introducing the thickness δ of the inner layer and the length scale b (Fig. 1B) defined as the elevation where $V = V_{max}/2$, the two-phase flow data are reported in Fig. 5C, where the results are compared with the characteristic height Y_{90} of the roller defined as the location where the void fraction C equals 0.90 as well as monophase wall jet data. The data showed an expanding shear zone (inner and outer layers) with increasing distance from the jump toe. The inner and outer layer length scales, δ and b respectively, were significantly larger than monophase flow observations.

The turbulent properties (Tu, T_{xx}) showed however some scale effects (Fig. 6) where Tu is the turbulent intensity: $Tu = v'/V$, v' is the root mean square of the longitudinal velocity component, and T_{xx} is the auto-correlation integral time scale. Herein Tu was calculated based upon the correlation analysis of the dual-tip probe signals [13,14]. In the air–water shear layer, the turbulence intensity was larger and the integral time scales were smaller for the largest Reynolds numbers, at the same given dimensionless location and for an identical Froude number. Fig. 6 includes also the distribution of auto-correlation time scales, indicating a monotonic increase in turbulent time scales with increasing distance from the invert. Further the bubble chord time distributions were not scaled according to a Froude similitude (Fig. 7). Comparatively larger bubble chord times were observed at low Reynolds numbers. This is seen in Fig. 7 presenting the normalised probability distribution functions of dimensionless bubble chord times. The present results supported the earlier findings [12,22], and they extended the findings to a broader range of air–water flow properties and Reynolds numbers.

3.1. Bubble cluster properties

When two bubbles are closer than a particular time/length scale, they can be considered a group of bubbles: i.e., a cluster. The characteristic water time/length scale may be related to the water chord statistics or to the near-wake of the preceding particle. Herein the latter approach was applied following CHANSON et al. [10] and Chanson [8]. Two bubbles were considered parts of a cluster when the water chord time between two consecutive bubbles was less than the lead bubble chord time. That is, when a bubble trailed the previous bubble by a short time/length, it was considered to be in the near-wake of and could be influenced by the leading particle.

The effects of the Reynolds number were also tested on the bubble clustering properties for $Fr_1 = 5.1$. Some results are shown in Fig. 8 in terms of the dimensionless number of clusters per second ($N_c\, d_1/V_1$), the percentage of bubble in clusters and the number of bubbles per cluster. The data indicated a relatively significant proportion of clustered bubbles, ranging from 26% to 42% (Fig. 8B). Importantly the dimensionless properties of bubble clusters in the air–water shear layers were not scaled according to a Froude similitude for $Fr_1 = 5.1$. The comparative analysis showed that the dimensionless number of clusters per second, the percentage of bubbles in cluster and the number of bubbles per clusters increased monotonically with the Reynolds number at a given dimensionless location $(x - x_1)/d_1$ and for a given Froude number $Fr_1 = 5.1$. This is seen in Fig. 8A–C.

In hydraulic jumps, the level of clustering may give a measure of the magnitude of bubble-turbulence interactions and associated energy dissipation. The present findings highlighted that the clustering affected a comparatively greater proportion of bubbles at high Reynolds numbers, indicating that the interactions between entrained bubbles and vortical structures were not scaled accurately with the Froude similarity.

4. Discussion

The Π-Buckingham theorem implied that only two dimensionless numbers are relevant to investigate air entrainment in hydraulic jumps using the same fluids in physical models and prototype (Eq. (4)). The selection of the Froude similitude was based upon some basic theoretical considerations [9,19,20]. A key feature of the hydraulic jump is the turbulent shear region. The jump toe is both a source of vorticity for the shear layer, as well as a source of entrapped air. The entrained 'bubbles' are convected in a region of high shear stress where bubble-turbulence interactions take place, including bubble breakup, vortex trapping of bubbles, bubble coalescence, modifications of vortical structures and of their properties. Since a Froude similarity was selected, the Reynolds number differed between the various physical models for an identical Froude number: i.e., the scaling ratio of the Reynolds number was equal to $L_{scale}^{3/2}$. In turn the scaling of turbulent shear stress tensor and vorticity vector differed from the velocity scaling ratio ($L_{scale}^{1/2}$ for a Froude similitude).

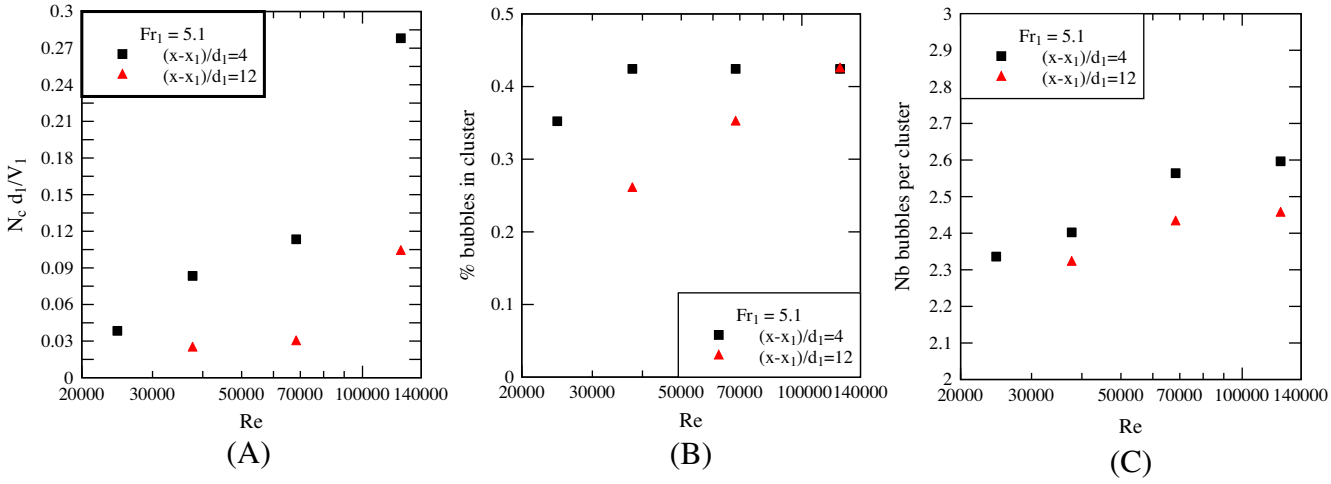

Fig. 8. Effects of the Reynolds number on the bubble cluster properties in the air–water turbulent shear layer of hydraulic jumps at the locations where $F = F_{max}$ ($y = y_{Fmax}$) – $Fr_1 = 5.1$, $(x - x_1)/d_1 = 4$ and 12. (A, Left) Dimensionless number of cluster per second $N_c \times d_1/V_1$. (B, Right) Percentage of bubbles in clusters. (C) Number of bubbles per cluster.

Table 2
Physical scaling of hydraulic jump with small inflow Froude number: basic recommendations.

Air–water flow property	Criterion to minimise scale effects	Remarks
Void faction (C)	$Re > 4 \times 10^4$	Self-similarity for $Re > 4 \times 10^4$
Time-averaged velocity (V)	$Re > 3 \times 10^4$	Self-similarity for $Re > 3 \times 10^4$
Bubble count rate (F)	$L_{scale} = 1$	Scale effects unless at full-sale
Bubble chord time (t_{ch})	$L_{scale} = 1$	Scale effects unless at full-sale
Turbulence intensity (Tu)	$L_{scale} = 1$	Scale effects unless at full-sale
Auto-correlation integral time scale (T_{xx})	$L_{scale} = 1$	Scale effects unless at full-sale
Bubble cluster properties	$L_{scale} = 1$	Scale effects unless at full-sale

Note: Experiments performed for $Fr_1 = 5.1$, $2.5 \times 10^4 \leqslant Re \leqslant 1.3 \times 10^5$ with air and Brisbane tap water.

The comparative analysis implied that, for hydraulic jumps with $Fr_1 = 5.1$, (a) the void fraction data obtained with Re < 40,000 could not be scaled up to $Re = 1 \times 10^5$ and (b) the bubble count rate data, turbulence properties, bubble chords and clustering properties with Reynolds numbers up to 125,000 could not be extrapolated to large-size prototype structures without significant scale effects in terms of bubble count rate, turbulence and bubble chord time distributions. The findings are summarised in Table 2 and they have some major implications of civil, environmental and sanitary engineering designs, because most hydraulic structures, storm water systems and water treatment facilities operate with Reynolds numbers within ranging from 10^6 to over 10^8.

For completeness, Chanson [6] tested the effect of the relative width W/d_1, with all other relevant parameters (Fr_1, Re, Mo) being constant. That is:

$$C, \frac{V}{V_1}, \frac{v'}{V_1}, \frac{F\,d_1}{V_1}, \frac{D_{ab}}{d_1}, \frac{N_c\,d_1}{V_1}, \ldots = f\left(\frac{W}{d_1}\right) \quad (7)$$

where the inflow Froude and Reynolds numbers were constant: i.e., $Fr_1 = 5.1$ and 8.5, Re = 70,000–95,000. The results showed that the relative channel width had no effect on the air–water flow properties at the centreline of the channel for $W/d_1 > 10$, including terms of the void fraction, bubble count rate and bubble chord time distributions. Since all the data tested in Table 1 satisfied $W/d_1 > 10$, the present results are believed also to be independent of the relative flume width.

5. Conclusion

The hydraulic jump is a complex phenomenon that remains incompletely understood. In the present study, a re-analysis of physical data was conducted with a focus on the air–water flow properties in hydraulic jumps with $Fr_1 = 5.1$. The Froude similarity was tested for a range of Reynolds numbers $2.5 \times 10^4 < Re < 1.3 \times 10^5$. The analysis was performed over a broad range of two-phase flow parameters including the distributions of void fraction, bubble count rate, velocity, turbulence intensity, integral time scale and bubble clustering properties. The comparative results demonstrated that, for hydraulic jumps with $Fr_1 = 5.1$, the void fraction data obtained with $Re < 4 \times 10^4$ could not be scaled up to $Re = 1 \times 10^5$. The bubble count rate data, turbulence properties, bubble chords and clustering properties with Reynolds numbers up to 1.25×10^5 would not be up-scaled to large-size prototype structures without significant scale effects in terms of bubble count rate, turbulence and bubble chord time distributions. The basic results are summarised in Table 2.

The findings have some implications of civil engineering, because most hydraulic structures operate at Reynolds numbers ranging from 10^6 to over 10^8. In a physical model, the flow conditions are said to be similar to those in the prototype flow conditions if the model displays similarity of form, similarity of motion and similarity of forces. The present results demonstrated quantitatively that the dynamic similarity of two-phase flows in hydraulic jumps at relatively small Froude numbers cannot be achieved with a Froude similarity unless working at full-scale.

Acknowledgment

The financial support of the Australian Research Council (Grants DP0878922 & DP120100481) is acknowledged.

References

[1] J.B. Bélanger, "Notes sur l'Hydraulique". ('Notes on Hydraulic Engineering'.) Ecole Royale des Ponts et Chaussées, Paris, France, 1841, session 1841–1842, 223p. (in French).
[2] P. Cain, I.R. Wood, Measurements of self-aerated flow on a spillway, Journal of Hydraulic Division, ASCE 107 (HY11) (1981) 1425–1444.

[3] Y. Chachereau, H. Chanson, Bubbly flow measurements in hydraulic jumps with small inflow froude numbers, International Journal of Multiphase Flow 37 (6) (2011) 555–564, http://dx.doi.org/10.1016/j.ijmultiphaseflow.2011.03.012.
[4] H. Chanson, Air Bubble Entrainment in Free-Surface Turbulent Shear Flows, Academic Press, London, UK, 1997. 401p.
[5] H. Chanson, The Hydraulics of Open Channel Flows: An Introduction, second ed., Butterworth-Heinemann, Oxford, UK, 2004. 630p.
[6] H. Chanson, Bubbly flow structure in hydraulic jump, European Journal of Mechanics B/Fluids 26 (3) (2007) 367–384, http://dx.doi.org/10.1016/j.euromechflu.2006.08.001.
[7] H. Chanson, Turbulent air–water flows in hydraulic structures: dynamic similarity and scale effects, Environmental Fluid Mechanics 9 (2) (2009) 125–142, http://dx.doi.org/10.1007/s10652-008-9078-3.
[8] H. Chanson, Convective transport of air bubbles in strong hydraulic jumps, International Journal of Multiphase Flow 36 (10) (2010) 798–814, http://dx.doi.org/10.1016/j.ijmultiphaseflow.2010.05.006.
[9] H. Chanson, Momentum considerations in hydraulic jumps and bores, Journal of Irrigation and Drainage Engineering ASCE 138 (4) (2012) 382–385. <http://dx.doi.org/10.1061/(ASCE)IR.1943-4774.0000409>.
[10] H. Chanson, S. Aoki, A. Hoque, Bubble entrainment and dispersion in plunging jet flows: freshwater versus seawater, Journal of Coastal Research 22 (3) (2006) 664–677. doi:10.2112/03-0112.1.
[11] H. Chanson, T. Brattberg, Experimental study of the air–water shear flow in a hydraulic jump, International Journal of Multiphase Flow 26 (4) (2000) 583–607.
[12] H. Chanson, C. Gualtieri, Similitude and scale effects of air entrainment in hydraulic jumps, Journal of Hydraulic Research, IAHR 46 (1) (2008) 35–44.
[13] H. Chanson, L. Toombes, Air–water flows down stepped chutes: turbulence and flow structure observations, International Journal of Multiphase Flow 28 (11) (2002) 1737–1761. ISSN 0301-9322.
[14] C. Crowe, M. Sommerfield, Y. Tsuji, Multiphase Flows with Droplets and Particles, CRC Press, Boca Raton, USA, 1998. 471p.
[15] D.A. Ervine, Air entrainment in hydraulic structures: a review, Proceedings of ICE – Water Maritime and Energy 130 (3) (1998) 142–153.
[16] W.K. George, H. Abrahamsson, J.E. Eriksson, R.I. Karlsson, L. Lofdahl, M. Wosnik, A similarity theory for the turbulent plane wall jet without external stream, Journal of Fluid Mechanics 425 (2000) 367–411.
[17] F.M. Henderson, Open Channel Flow, MacMillan Company, New York, USA, 1966.
[18] J.W. Hoyt, R.H.J. Sellin, Hydraulic jump as 'mixing layer', Journal of Hydraulic Engineering, ASCE 115 (12) (1989) 1607–1614.
[19] J.A. Liggett, Fluid Mechanics, McGraw-Hill, New York, USA, 1994.
[20] J. Lighthill, Waves in Fluids, Cambridge University Press, Cambridge, UK, 1978. 504p.
[21] J.S. Montes, Hydraulics of Open Channel Flow, ASCE Press, New-York, USA, 1998. 697p.
[22] F. Murzyn, H. Chanson, Experimental assessment of scale effects affecting two-phase flow properties in hydraulic jumps, Experiments in Fluids 45 (3) (2008) 513–521, http://dx.doi.org/10.1007/s00348-008-0494-4.
[23] P. Novak, J. Cabelka, Models in Hydraulic Engineering. Physical Principles and Design Applications, Pitman Publ., London, UK, 1981.
[24] N. Rajaratnam, The hydraulic jump as a wall jet, Journal of Hydraulic Division ASCE 91 (HY5) (1965) 107–132.
[25] N. Rajaratnam, Hydraulic Jumps, in: V.T. Chow (Ed.), Advances in Hydroscience, vol. 4, Academic Press, New York, USA, 1967, pp. 197–280.
[26] N. Rajaratnam, Turbulent Jets, vol. 5, Elsevier Scientific, Development in Water Science, New York, USA, 1976.
[27] N.S.L. Rao, H.E. Kobus, Characteristics of Self-Aerated Free-Surface Flows, Water and Waste Water/Current Research and Practice, vol. 10, Eric Schmidt Verlag, Berlin, Germany, 1971.
[28] H. Rouse, T.T. Siao, S. Nagaratnam, Turbulence characteristics of the hydraulic jump, Transactions, ASCE 124 (1959) 926–950.
[29] M.F. Tachie, R. Balachandar, D.J. Bergstrom, Roughness effects on turbulent plane wall jets in an open channel, Experiments in Fluids 37 (2004) 281–292.
[30] I.R. Wood, Air Entrainment in Free-Surface Flows IAHR Hydraulic Structures Design Manual No. 4, Hydraulic Design Considerations, Balkema Publ., Rotterdam, The Netherlands, 1991. 149p.